AGU PUBLICATIONS

JGR

Journal of Geophysical Research: Atmospheres

RESEARCH ARTICLE
10.1002/2016JD025430

**Key Points:**
- Circulation patterns adjust to a negative radiative perturbation to counterbalance the heat anomaly
- Asian aerosols cannot explain the intensification of trade wind anomalies linked to the hiatus
- Asian aerosol emissions are an inadequate explanation for the recent stabilization of GMST

**Correspondence to:**
L. B. Kuntz,
lkuntz@fas.harvard.edu

**Citation:**
Kuntz, L. B., and D. P. Schrag (2016), Impact of Asian aerosol forcing on tropical Pacific circulation and the relationship to global temperature trends, *J. Geophys. Res. Atmos.*, *121*, 14,403–14,413, doi:10.1002/2016JD025430.

Received 27 MAY 2016
Accepted 28 NOV 2016
Accepted article online 7 DEC 2016
Published online 22 DEC 2016

©2016. American Geophysical Union. All Rights Reserved.

# Impact of Asian aerosol forcing on tropical Pacific circulation and the relationship to global temperature trends

**L. B. Kuntz**[1] **and D. P. Schrag**[1]

[1]Department of Earth and Planetary Sciences, Harvard University, Cambridge, Massachusetts, USA

**Abstract** The recent slowdown in the warming of global surface temperatures has been linked to the enhancement of trade winds in the central equatorial Pacific. The possible role of Asian aerosol emissions in forcing these wind anomalies is investigated through a series of idealized model simulations. Circulation patterns in response to localized negative radiative perturbations, indicative of aerosol effects, are investigated for both a slab and an active ocean models. The results suggest that Asian aerosols cannot explain the recent intensification of trade wind anomalies in the equatorial Pacific.

## 1. Introduction

Since 1890, the rise in global mean surface temperatures (GMSTs) has been dominated by two periods of rapid increase, from 1910 to 1944 and 1976 to 2002, interspersed with two periods of relative stability, from 1944 to 1975 and from 2002 to the present day. The recent stabilization of GMST has been deemed a "hiatus" [*Trenberth and Fasullo*, 2013], although there has been some discussion surrounding the statistical significance of this "pause" [*Cowtan and Way*, 2014; *Karl et al.,* 2015]. Even if temperatures are still rising, the rate of warming has clearly slowed since 2002 as compared to the prior two and a half decades [*Fyfe et al.,* 2016]. These alternations between rapid warming and relative stability over the past century suggest that a common physical mechanism may be at play. A few studies have highlighted the Pacific Decadal Oscillation, or PDO, as the possible cause behind the current hiatus [*Meehl et al.,* 2011; *Balmaseda et al.,* 2013; *Meehl et al.,* 2013]. The PDO is characterized by a pattern of sea surface temperatures in the tropical and subtropical Pacific that oscillates on decadal timescales between warm tropics with cool subtropics (positive PDO) and cool tropics and warm subtropics (negative PDO). During both periods of surface temperature stability the PDO was in a negative phase, although the periods of rapid warming corresponded with a positive PDO [*Trenberth and Fasullo*, 2013; *Tollefson*, 2014]. The midcentury hiatus, however, has been attributed to increases in aerosol forcing. Between the 1940s and 1970s, sulfate aerosol emissions drastically increased as the use of coal for electricity generation grew in the United States and Europe. These aerosols are thought to have added a negative climate forcing through the reflection of incoming solar radiation and the alteration of cloud microphysics, which counterbalanced increasing levels of greenhouse gases [*Bryson*, 1974; *Broecker*, 1975; *Bryson and Wendland*, 1975; *Bolin and Charlson*, 1976]. Support for the attribution of the midcentury hiatus to aerosol forcing came from improvements seen in the ability of models to replicate the historical temperature record upon the addition of an aerosol forcing [*Mitchell et al.,* 1995; *Santer et al.,* 1995], hemispheric differences in emissions and cooling trends [*Damon and Kunen*, 1976], and changes in the diurnal temperature range [*Wild et al.,* 2007]. In addition, aerosols have been shown to drive multidecadal sea surface temperature changes in the North Atlantic and North Pacific [*Boo et al.,* 2015; *Booth et al.,* 2012], the frequency of Atlantic hurricanes [*Dunstone et al.,* 2013], and the South Asian summer monsoon [*Bollasina et al.,* 2011], highlighting their importance to circulation patterns.

Given that aerosol forcing is a widely accepted mechanism for explaining the stability of midcentury temperatures, it is reasonable to ask whether aerosol emissions are also responsible for the recent stabilization of GMST. Coal burning in China over the past two decades has led to a dramatic increase in Asian aerosol emissions, such as sulfur dioxide (Figure 1) [*Smith et al.,* 2011]. Although Asian sulfate aerosol emissions have increased steadily since 1970, the stabilization of GMST occurred around 2000. The offset of these two timelines does not negate the possibility of an Asian aerosol forcing, as it is not just the magnitude of emissions but also the spatial and temporal distribution, transport, and interactions with clouds that impact the response [*Carslaw et al.*, 2013]. These factors have changed over the period of Asian aerosol emission

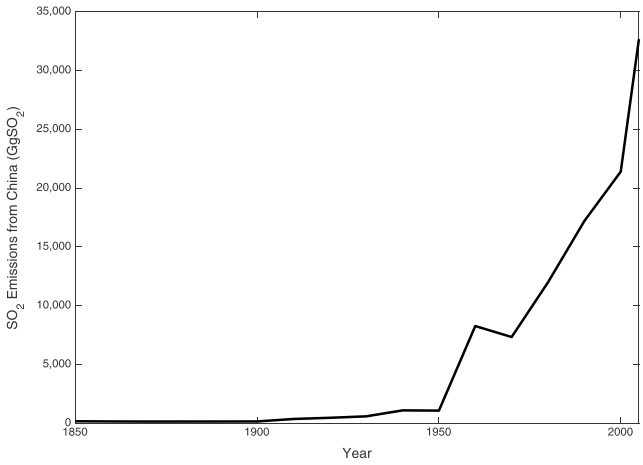


**Figure 1.** Chinese sulphur dioxide emissions over time [*Smith et al*., 2011].

increases, evident in the corresponding decline of European and North American aerosol emissions [*Kinne et al.,* 2013], obscuring the translation of emissions to an exact forcing magnitude. A number of studies using in situ measurements, satellite data, ground-based observations, and modeling simulations have estimated the combined localized direct and indirect forcing from Asian aerosols to be between $-8$ and $-30\,\mathrm{W\,m^{-2}}$ [*Ramanathan et al.,* 2001; *Markowicz et al.,* 2003; *Yabe et al.,* 2003; *Bates et al.,* 2006; *Wang et al.,* 2014]; however, the radiative impact of aerosols remains uncertain [*Hansen et al.,* 2011; *Carslaw et al.,* 2013].

Aerosols could explain the stabilization of GMST simply through the reduction of the top of the atmosphere energy imbalance. Yet attribution of the recent trend in GMST to aerosol forcing requires additional evidence, such as an explanation for the spatial patterns of temperature and winds that have been linked to the hiatus. Patterns of sea surface temperature (SST) anomalies and wind trends in the tropical Pacific Ocean have stood out in addition to the deviation in the global warming trend since 2002. Models overestimate the warming over the past decade, particularly in the eastern Pacific where the disagreement between observed and modeled temperature trends is largest [*England et al.,* 2014]. This region, however, is critical to controlling global climate—*Kosaka and Xie* [2013] were able to recreate the hiatus in a model by fixing SSTs in the eastern Pacific to match observations. Their findings highlight the importance of accurately capturing the tropical Pacific when it comes to simulating global temperatures. Yet to replicate the temperature pattern in this region, surface trade winds are critical. *England et al.* [2014] analyzed wind stress trends between 1992 and 2012 and suggested that a recent strengthening of equatorial trade winds explains the cool state of the eastern Pacific tied to the hiatus. Rather than trends, the difference in mean surface wind fields during and prior to the hiatus is a more natural metric for the change in state of the tropical Pacific. As shown in Figure 2, the difference in mean winds shows a similar strengthening along the equatorial Pacific as noted by *England et al.* [2014]. This posits that a deeper understanding of the hiatus lies in better understanding of trade winds. *Takahashi and Watanabe* [2016] suggested that aerosol forcing explains some of the intensification of the trade winds but not the trends in GMST. Their analysis, however, found the intensification of trades farther westward in the tropical Pacific than observed by *England et al.* [2014] and considered the combined effect of all changes in aerosol emissions since preindustrial as opposed to isolating the effects of recent changes in regional emissions. If the recent increase in Asian aerosol emissions is the physical mechanism behind the stabilization of GMST, the negative radiative forcing from these emissions must also explain the observed wind trends.

This study examines the connection between enhanced Asian aerosol emissions and the wind anomalies associated with the current hiatus. Climate model simulations are performed with a negative radiative forcing over Eastern Asia to simulate Asian aerosol effects. The effect of aerosols transported over the Pacific is also considered, as there is evidence of increasing trends in aerosol outflow from Asia [*Yang et al.,* 2015] and increasing aerosol loads in this region could have a significant impact due to the heightened sensitivity of indirect aerosol forcing in pristine environments [*Carslaw et al.,* 2013]. Because there is such large uncertainty surrounding the interactions of aerosols with clouds and radiation, we have not sought to simulate the exact forcing pattern of Asian aerosols. Rather, we have asked how a shortwave radiation anomaly, suggestive of aerosol effects, would impact circulation patterns in the tropical Pacific. As the circulation response to heating

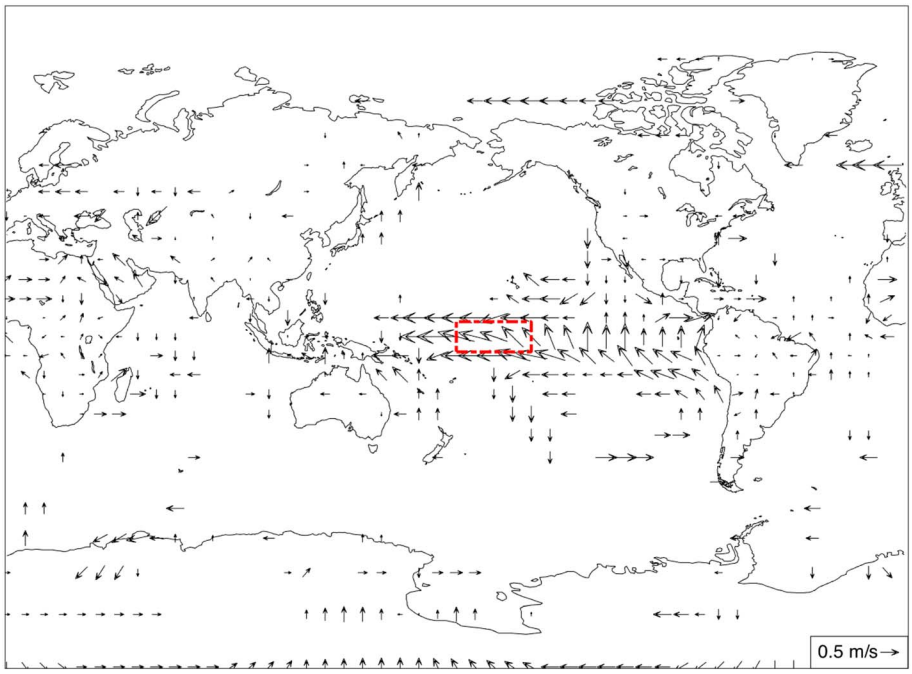


**Figure 2.** The difference in mean surface winds between the hiatus (2002–2012) and the period prior (1989–2001) from the European Centre for Medium-Range Weather Forecasts (ECMWF) Re-Analysis (ERA-Interim) [*Dee et al.,* 2011]. The red box denotes the region in the equatorial Pacific where *England et al.* [2014] noted the largest trade anomalies (6°S–6°N, 180°W–150°W). Only statistically significant differences in mean surface winds are shown based on a *t* test with 95% confidence level.

anomalies is sensitive to the forcing location [*Branstator*, 1985; *Meehl et al.,* 2006], a couple of different simulations are performed to investigate the impact of the location and extent of a radiative forcing on model response. Our objective is to assess whether a negative radiative anomaly could reproduce the observed strengthening of trade winds that has been tied to the hiatus.

## 2. Methods

The magnitude of aerosol forcing is marked by large uncertainty for both the direct and indirect effects due to the nuanced interactions between aerosol distributions, radiation, and clouds [*Boucher et al.,* 2013]. Although refining these uncertainties and imposing realistic sulfate aerosol effects is important when evaluating the full impact of Asian aerosols, the aim of this work is to broadly examine the potential influence of aerosols on large-scale circulation patterns over the Pacific. To this end, modifying the solar forcing may be an acceptable idealization of aerosols' combined direct and indirect effects, as atypical circulations are largely driven by anomalous energy fluxes. Mimicking sulfate aerosol forcing by reducing the solar constant is often used in investigations of geoengineering impacts [*Govindasamy and Caldeira*, 2000; *Govindasamy et al.,* 2002, 2003; *Matthews and Caldeira*, 2007; *Kravitz et al.,* 2013], with this simplification producing similar climate states as a modeled addition of aerosols [*Kalidindi et al.,* 2015]. Using the Community Earth System Model (CESM) from the National Center for Atmospheric Research, the solar constant is selectively modified over a portion of the globe. The modification to the solar constant of $-78\,\mathrm{W\,m^{-2}}$ was selected, such that once the albedo effect and diurnal average are considered, the local forcing is within this range of estimates of past studies [*Ramanathan et al.,* 2001; *Markowicz et al.,* 2003; *Yabe et al.,* 2003; *Bates et al.,* 2006; *Wang et al.,* 2014] and on the order of $-10\,\mathrm{W\,m^{-2}}$. Although the focus is on reflective aerosols, the presence of any adsorptive aerosols, such as black carbon, can be viewed as a decrease in the strength of the forcing, as the reflective and adsorptive aerosols have a similar structure of tropospheric response but of opposite signs [*Xu and Xie*, 2015]. The forcing idealization inherently overlooks the fine details of aerosols, such as changes in precipitation and latent heating as well as the vertical distribution of the forcing; however, it provides the simplest picture possible that still captures dominant changes in the circulation.

Three different perturbation patterns are investigated and summarized in Table 1. In the first, the modification to the solar constant is applied in the region of maximum observed aerosol optical depth [*Kinne et al.,*

**Table 1.** Model Simulation Configurations[a]

| Simulation Name | Ocean | Solar Forcing Perturbation | Perturbed Area |
|---|---|---|---|
| S-Control | Slab | - | - |
| S-Solar | Slab | $-78\ W\ m^{-2}$ | 15°N–35°N, 105°E–125°E |
| S-Solar2A | Slab | $-78\ W\ m^{-2}$ | 15°N–35°N, 105°E–145°E |
| S-SolarP | Slab | $-78\ W\ m^{-2}$ | 25°N–40°N, 140°E–200°E |
| A-Control | Active | - | - |
| A-SolarP | Active | $-78\ W\ m^{-2}$ | 25°N–40°N, 140°–200°E |

[a]The solar constant (here $1361.27\ W\ m^{-2}$) is modified over the specified region by the solar forcing perturbation.

2013]. As cold fronts and orographic lifting transport aerosols over the Pacific [*Liu et al.,* 2003], the second configuration extends the perturbation eastward. Finally, the impact of a radiative anomaly over the Pacific Ocean is considered. The location of the perturbation was chosen to align with transport pathways of Asian aerosols identified in previous studies [*Jaffe et al.,* 1999; *Liu et al.,* 2003].

The simulations are run on a 2° grid, with present-day forcings, and an atmospheric $CO_2$ concentration of 400 ppm. For the atmosphere component of CESM, the Community Atmosphere Model version 4.0 is used. A slab ocean model is used for all forcing configurations. The perturbation over the Pacific Ocean is also run with a fully active ocean model—the Parallel Ocean Program version 2 (POP2)—to understand the complete effects of ocean-atmosphere feedback on the circulation response. Control simulations, without any modification to the solar constant, are run using both the slab and active ocean configurations. For both control and perturbation cases, the model is spun up for 16 years, followed by 20 years of simulation with monthly averaged output.

## 3. Results

Figure 3 shows the time-averaged atmospheric surface temperature and wind response to the various perturbations. For all three slab ocean simulations, the region of the perturbation (designated by a black bounding box for clarity) corresponds to the region of maximum cooling. A box is also placed around the region in the equatorial Pacific where *England et al.* [2014] noted the largest enhancement of easterly trade wind anomalies during the hiatus. Although the wind response in all cases is indicative of an anticyclonic circulation about a high-pressure cell in the region of the perturbation, these wind anomalies do not appear to reach the equatorial region highlighted by *England et al.* [2014]. As the perturbation over the Pacific (S-SolarP) has a stronger easterly wind response in the central and western Pacific than the other two simulations, the subsequent focus is placed on understanding the complete response in this setup. The broad picture of the circulation response in this simulation should be extendable to the other configurations even though the details of the circulation response will be case specific.

With a slab ocean model, the development of a high in the region of the perturbation is evident at the surface but disappears at higher levels in the atmosphere (Figure 4). Although the wind response in the upper levels of the atmosphere is in geostrophic balance with the pressure field, the surface winds deviate from contours of constant pressure, reminiscent of the frictional effects seen in an Ekman layer. Overall, the spatial structure of the pressure and wind response enhances the mean state high over the Pacific rather than aligning with the region of the imposed perturbation.

The responses of the zonal mean velocities to the S-SolarP simulation are largely restricted to the Northern Hemisphere (Figure 5). The jet stream in the Northern Hemisphere strengthens and shifts equatorward in response to the perturbation. Simultaneously, the meridional velocity exhibits greater poleward transport in the upper levels of the atmosphere and greater equatorward transport near the surface. The vertical velocity shows enhanced upwelling in the southern tropics and enhanced downwelling in the northern tropics.

Figure 3d shows the response to the Pacific perturbation with a fully active ocean model. Although the temperature, surface pressure, geopotential height, and wind response patterns are similar to the slab ocean simulation, the magnitude of the response is damped (Figures 6 and 7). The temperature response has a smaller magnitude and hemispheric gradient than with the slab ocean (Figure 3c). Similarly, with the active ocean the high surface pressure localized in the region of the perturbation is diminished and the wind response is substantially dampened. The jet stream in the Northern Hemisphere still shows an equatorward

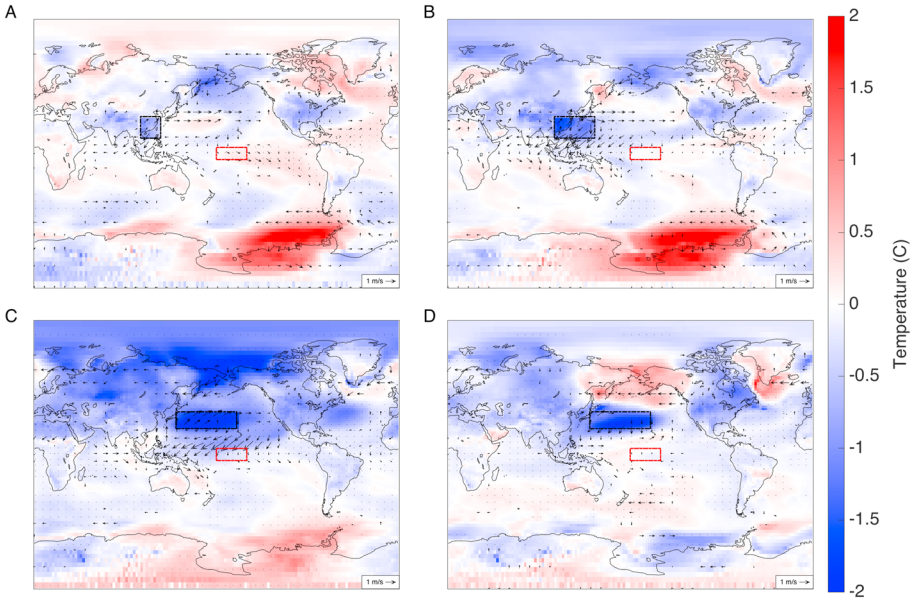


**Figure 3.** The time-averaged atmospheric surface temperature (shading) and wind (vector) anomaly response in the (a) S-Solar simulation, (b) S-Solar2A simulation, (c) S-SolarP simulation, and (d) A-SolarP simulation. The black bounding box denotes the region where the perturbation to the solar constant was applied and the red bounding box denotes the region in the equatorial Pacific where *England et al.* [2014] noted the largest trade wind anomalies. A *t* test was performed to determine statistically significant anomalies at the 95% confidence level. Stippling indicates where surface temperature anomalies are significant, and only significant wind anomalies are shown.

shift and intensification with the POP2 ocean model; however, a response in meridional and vertical velocities is less coherent than with the slab ocean model.

The differences in surface heat flux response between the active and slab ocean simulations are illustrated in Figure 8 for sensible and latent heat. The active ocean simulation exhibits an enhanced heat flux response from the ocean to the atmosphere as compared to the slab ocean. In the localized region about the

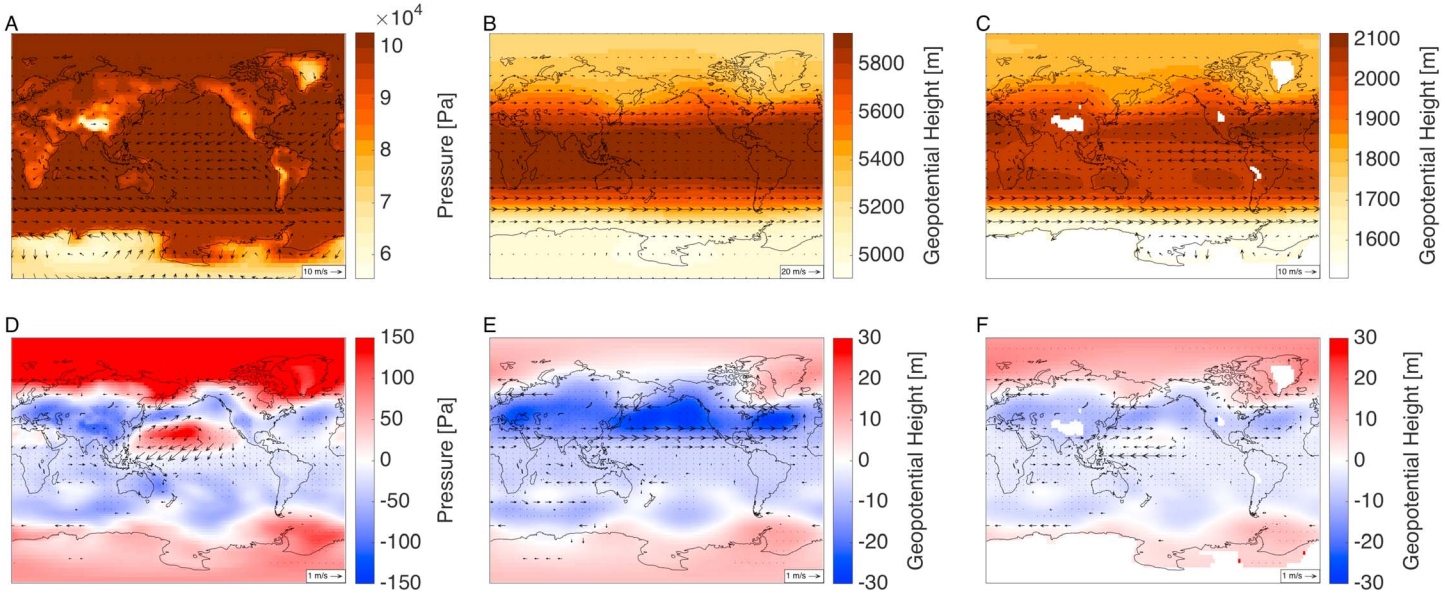


**Figure 4.** Slab ocean climatology and circulation response in the S-SolarP simulation. Surface pressure (shading) and surface winds (vectors) from (a) the slab ocean control climatology and (d) the anomalous response. Geopotential height (shading) and winds (vectors) at of the climatology and anomalous response at (b and e) 500 mp and (c and f) 800 mp. A *t* test was performed to determine statistically significant anomalies at the 95% confidence level. Stippling indicates where surface pressure and geopotential height anomalies are significant, and only significant wind anomalies are shown.

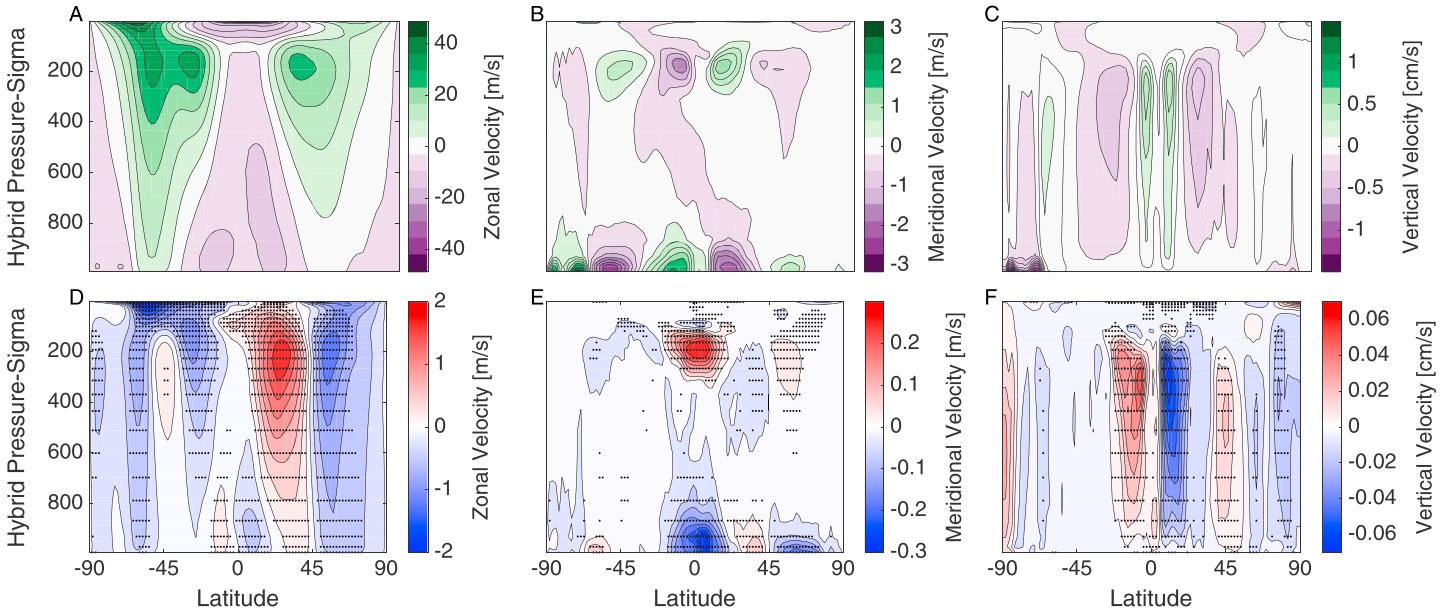


**Figure 5.** Zonally averaged slab ocean climatology and anomalous response in the S-SolarP simulation for (a and d) zonal velocity, (b and e) meridional velocity, and (c and f) vertical velocity. Stippling indicates where anomalies are significant to a 95% confidence level from a *t* test analysis.

perturbation, the increase of both sensible and latent heat fluxes with the active ocean is evident, with the magnitude of the latent heat flux dominating the overall response.

## 4. Discussion

Regardless of the location of the perturbed region, all of the model runs exhibit the same general features of local cooling and anticyclonic circulation within the region of the forcing. For both the S-Solar and S-Solar2A cases, the wind response is too far westward to correspond to the region in the central Pacific observed to have the largest enhancement of easterly winds [*England et al.,* 2014]. As the perturbation over the Pacific

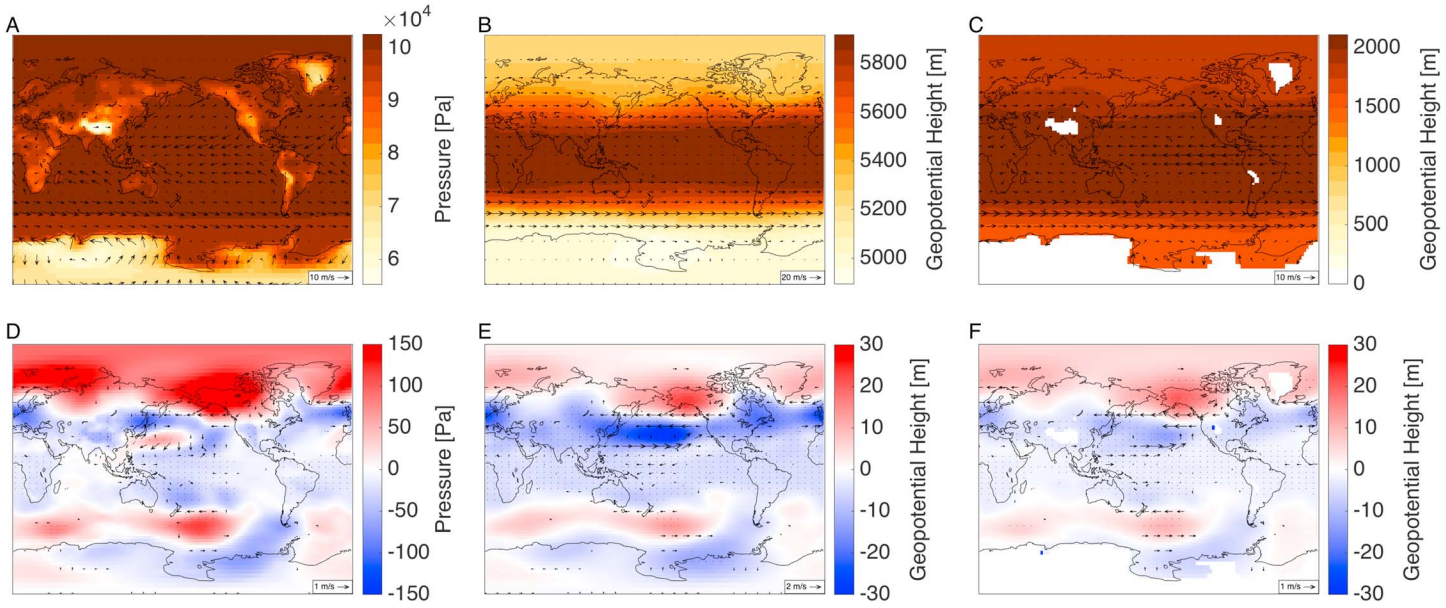


**Figure 6.** Active ocean climatology and circulation response in the A-SolarP simulation. Surface pressure (shading) and surface winds (vectors) from (a) the slab ocean control climatology and (d) the anomalous response. Geopotential height (shading) and winds (vectors) at of the climatology and anomalous response at (b and e) 500 mp and (c and f) 800 mp. A *t* test was performed to determine statistically significant anomalies at the 95% confidence level. Stippling indicates where surface pressure and geopotential height anomalies are significant, and only significant wind anomalies are shown.

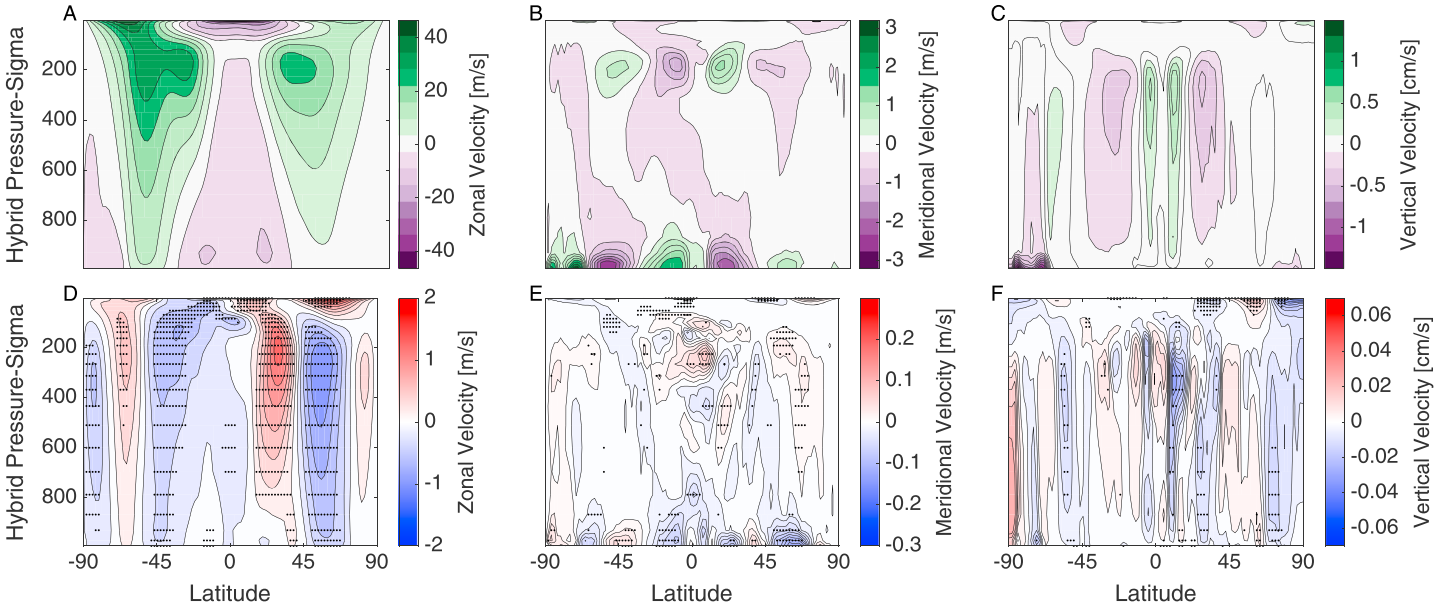


**Figure 7.** Zonally averaged active ocean climatology and anomalous response in the A-SolarP simulation for (a and d) zonal velocity, (b and e) meridional velocity, and (c and f) vertical velocity. Stippling indicates where anomalies are significant to a 95% confidence level from a *t* test analysis.

(S-SolarP and A-SolarP) shows a mild enhancement of easterly winds in the region corresponding to observations, the majority of the discussion will focus on understanding the dynamics of the response in this case, with the intent that the broad picture of the response is extendable to the other cases.

Overall, the circulation responds to balance the negative radiative perturbation through adjustments in heat transport. In the slab ocean simulation, the heat adjustment is largely confined to the atmosphere due to the restriction of heat transport between the deep and surface ocean. The Hadley cell can shift to counteract hemispheric energy imbalances [*Kang et al.,* 2008]. Decreasing the incoming radiation in the Northern Hemisphere subtropics establishes an energy imbalance. Thus, to maintain the mean climate state in response to the negative perturbation, the Hadley cell shifts southward and increases heat transport to the northern subtropics. This adjustment of the Hadley cell is evident in the velocity profiles, which show increased meridional velocity in the upper branch of the northern Hadley cell and enhanced downwelling in the northern subtropics (Figures 7d–7f).

The mean circulation pattern in the Northern Hemisphere appears to contract equatorward in response to the perturbation. In the upper levels of the atmosphere, the geopotential height anomalies follow a similar pattern to the mean geopotential height of the control state, with a high anomaly over the North Pole bordered by a region of depressed geopotential height (Figure 6). The similarity of the anomaly and mean state patterns suggests a meridional shift in the mean state. An equatorward shift of the jet stream is evident in the Northern Hemisphere, as shown in changes in zonal velocity (Figure 6d). This shift can be understood simply as a response to changes in the equator-to-pole temperature gradient associated with the perturbation. To first order, the location of the jet stream is dictated by a balance between the equatorward Coriolis force and the poleward pressure gradient. As the radiative perturbation diminishes the midlatitude temperature gradient, and consequentially the pressure gradient, the wind fields respond accordingly, shifting the jet stream southward.

The atmospheric response for the active ocean is similar to the slab ocean, although with diminished magnitude as the ocean plays a larger role in the heat transport adjustment. Heat adjustment in response to the perturbation is no longer suppressed with an active ocean, decreasing the burden placed on the atmospheric response. As compared to the slab ocean, the heat flux adjustment from the ocean to the atmosphere is substantially stronger in the active ocean, particularly for the latent heat flux (Figure 8).

The ocean and atmosphere respond to counteract the negative radiative forcing through enhanced heat transport, and the strengthening of surface trade winds is evident. The location of the wind response,

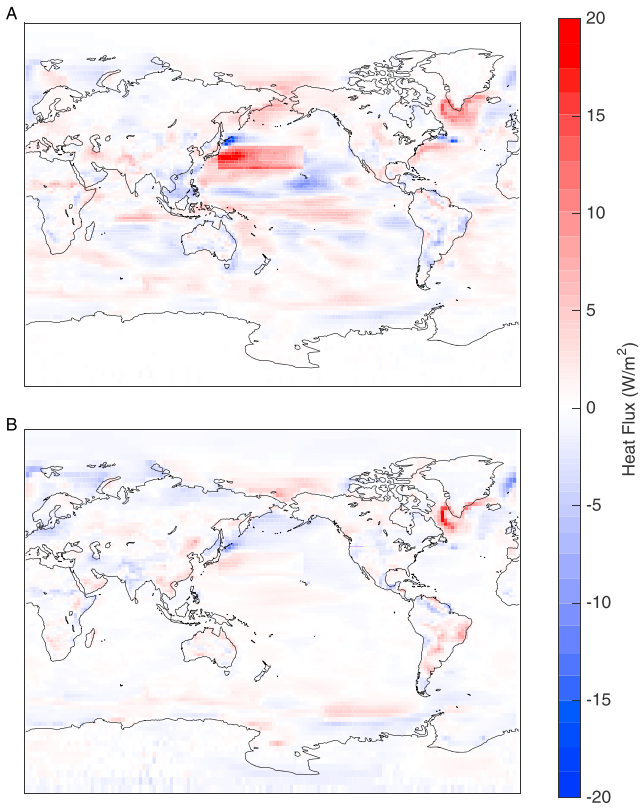


**Figure 8.** The difference in the surface (a) latent and (b) sensible heat flux anomaly between the A-SolarP and S-SolarP simulations.

however, is northward of the observed fields linked to the hiatus. Both the slab and active ocean configurations show an enhancement of winds in the region of the perturbation, yet there is little impact on equatorial wind anomalies. Even if the perturbation were farther southward, it is doubtful that the circulation response would reach the equator. Moving the perturbation closer to the equator would likely dampen the Hadley circulation. As the dominant response to the simulated anomalies is the adjustment of heat transport to counterbalance the perturbation, a tropical radiative forcing would lead to an atmosphere that decreases meridional transport to reduce heat loss. Upwelling in the Hadley cell would decrease, and the overall circulation would weaken. Rather than strengthening the equatorial trade winds, as observed in connection with the hiatus, this would weaken the winds. In addition, the Coriolis effect in the tropics is weaker than in the midlatitudes. Thus, a wind response to a pressure anomaly would have a larger component perpendicular to pressure contours, as opposed to tangential. To replicate the enhancement of trade winds, a low pressure in the western tropical Pacific and/or high pressure in the eastern tropical Pacific would likely be necessary—the inverse of what one would expect from enhanced Asian aerosol forcing. There is no evidence of an aerosol source in such locations as to explain the observed atmospheric trends. The lack of correspondence between the wind patterns in response to the perturbation and the observed trends indicates that a negative radiative forcing over the Pacific is not responsible for these patterns. Although the simulated forcing is a highly idealized representation of Asian aerosols, it casts doubt upon the role Asian aerosols play in explaining the current hiatus.

The idealization of an aerosol forcing through a perturbation of the solar constant is coarse, missing the intricacies of the forcing. For instance, a constant perturbation to the solar constant leads to a seasonally varying forcing as the length of day and solar declination change. This causes variations in the forcing of 25% over the seasonal cycle, with a maximum in summer and minimum in winter—opposite the observed Asian aerosol loading patterns, which peak in winter [*Liu et al.,* 2003]. In addition, the idealization glosses over the vertical forcing structure, transport pathways, and chemical interactions. Despite these shortcomings, investigating the response to such a radiative perturbation still provides insight on the effects of Asian aerosols. The

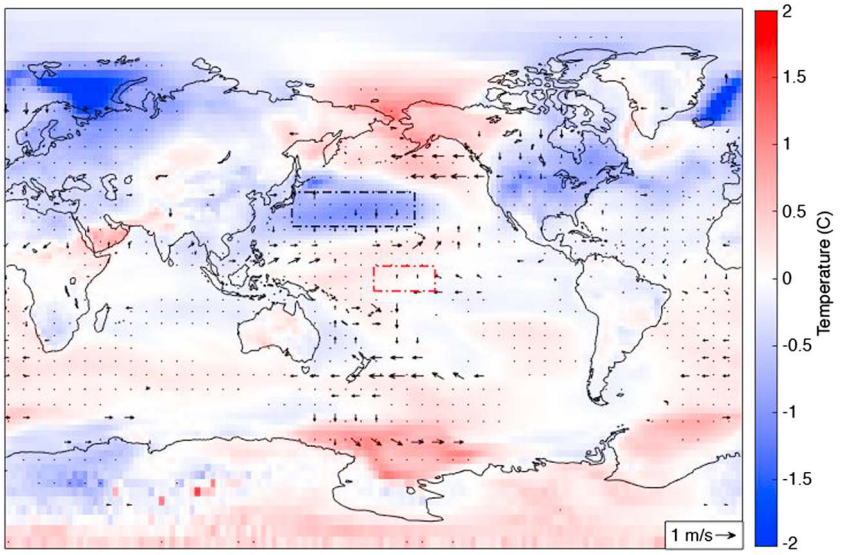


**Figure 9.** The time-averaged atmospheric surface temperature (shading) and wind (vector) anomaly response to a simulation with increased sulphate aerosol concentrations. Monthly sulphate concentrations over the Pacific are increased tenfold compared to 2000 levels in all atmospheric levels. The black bounding box denotes the region where the perturbation to the sulphate aerosol was applied, and the red bounding box denotes the region in the equatorial Pacific where *England et al.* [2014] noted the largest trade wind anomalies. A *t* test was performed to determine statistically significant anomalies at the 95% confidence level. Stippling indicates where surface temperature anomalies are significant, and only significant wind anomalies are shown.

inclusion of the finer details of aerosol effects does not change the overall response. Increasing sulphate aerosol loading by an order of magnitude over the Pacific produces temperature and wind response patterns similar to the idealized aerosol forcing (Figure 9). A more realistic aerosol representation does not change the overall conclusion about aerosol forcing on large-scale circulation patterns: the atmospheric adjustment to increase heat transport in response to a midlatitude negative radiative perturbation cannot evoke a substantial response in equatorial wind patterns.

These results contradict the conclusions of *Takahashi and Watanabe* [2016], who attributed part of the recent equatorial wind trends to aerosols. *Takahashi and Watanabe* [2016] compared a model with all climate forcings to a model with aerosols prescribed to preindustrial levels. They found that including aerosols did strengthen equatorial Pacific trade winds, but the magnitude of change in wind speed was only a third of what has been observed. Moreover, it is not clear how much of the wind changes can be attributed to aerosol changes from the 1990s to the hiatus period, as their comparison was based on a preindustrial base state. In our analysis, we consider changes in Asian aerosols, which are the major source of change from the 1990s to the hiatus period and would be most likely to impact circulation.

Our finding that Asian aerosols are unable to explain the current hiatus raises questions as to the attribution of the midcentury hiatus to anthropogenic aerosol forcing. Although this study does not simulate the effects of aerosols in the geographical locations tied to the midcentury hiatus, the similarities between the two periods of temperature stability, in particular the phase of the PDO, suggest a common underlying mechanism. Unless one argues that aerosols were driving the PDO during the midcentury but are not doing so currently, or that the correlation between the phase of the PDO and the hiatus periods is purely coincidental, then it suggests that sulfate aerosols were not the primary factor behind either hiatus period.

## 5. Conclusion

We have explored whether Asian aerosols can explain the recent enhancement of equatorial trade winds tied to the hiatus. Model experiments with the Asian aerosol forcing idealized as a negative radiative perturbation were performed to investigate the circulation response. The overall circulation adjusts to counterbalance the perturbation through enhanced heat transport but does not replicate the observed equatorial wind patterns during the hiatus period. This indicates that Asian aerosol emissions are not an adequate explanation for the

recent plateau in GMST. The inability of an idealized Asian aerosol forcing to replicate key circulation patterns also suggests the need to reexamine the attribution of the midcentury hiatus to aerosol forcing.

**Acknowledgments**
This material is based upon work supported by a National Science Foundation Graduate Research Fellowship (grant DGE1144152) to L.B.K. The modeling results for this paper are available by contacting the corresponding author L. Kuntz (lkuntz@fas.harvard.edu). All observational data in this paper are properly cited and referred to within the reference list.

## References

Balmaseda, M. A., K. E. Trenberth, and E. Källén (2013), Distinctive climate signals in reanalysis of global ocean heat content, *Geophys. Res. Lett.*, *40*, 1–6, doi:10.1002/grl.50382.

Bates, T. S., et al. (2006), Aerosol direct radiative effects over the northwest Atlantic, northwest Pacific, and North Indian Oceans: Estimates based on in-situ chemical and optical measurements and chemical transport modeling, *Atmos. Chem. Phys.*, *6*, 1657–1732, doi:10.5194/acp-6-1657-2006.

Boucher, O., et al. (2013), Clouds and aerosols, in *Climate Change 2013: The Physical Science Basis. Contribution of Working Group I to the Fifth Assessment Report of the Intergovernmental Panel on Climate Change*, edited by T. F. Stocker et al., pp. 571–657, Cambridge Univ. Press, Cambridge, U. K.

Bolin, B., and R. J. Charlson (1976), On the role of the tropospheric sulfur cycle in the shortwave radiative climate of the Earth, *Ambio*, *5*, 47–54.

Bollasina, M. A., Y. Ming, and V. Ramaswamy (2011), Anthropogenic aerosols and the weakening of the South Asian summer monsoon, *Science*, *334*, 502–505, doi:10.1126/science.1204994.

Boo, K.-O., B. B. B. Booth, Y.-H. Byun, J. Lee, C. Cho, S. Shim, and K.-T. Kim (2015), Influence of aerosols in multidecadal SST variability simulations over the North Pacific, *J. Geophys. Res. Atmos.*, *120*, 517–531, doi:10.1002/2014JD021933.

Booth, B. B. B., N. J. Dunstone, P. R. Halloran, T. Andrews, and N. Bellouin (2012), Aerosol implicated as a prime driver of twentieth-century North Atlantic climate variability, *Nature*, *484*, 228–232, doi:10.1038/nature10946.

Branstator, G. (1985), Analysis of general circulation model sea-surface temperature anomaly simulations using a linear model. Part I: Forced solutions, *J. Atmos. Sci.*, *42*, 2225–2241, doi:10.1175/1520-0469(1985)042.

Broecker, W. S. (1975), Climatic change: Are we on the brink of a pronounced global warming?, *Science*, *189*, 460–463, doi:10.1126/science.189.4201.460.

Bryson, R. A. (1974), A perspective on climatic change, *Science*, *184*, 753–760, doi:10.1126/science.184.4138.753.

Bryson, R. A., and W. A. Wendland (1975), Climatic effects of atmospheric pollution, in *The Changing Global Environment*, edited by S. F. Singer, pp. 139–147, Springer, Boston.

Carslaw, K. S., et al. (2013), Large contribution of natural aerosols to uncertainty in indirect forcing, *Nature*, *503*, 67–71, doi:10.1038/nature12674.

Cowtan, K., and R. G. Way (2014), Coverage bias in the HadCRUT4 temperature series and its impact on recent temperature trends, *Q. J. R. Meteorol. Soc.*, *140*, 1935–1944, doi:10.1002/qj.2297.

Damon, P. E., and S. M. Kunen (1976), Global cooling?, *Science*, *193*, 447–453, doi:10.1126/science.193.4252.447.

Dee, D. P., et al. (2011), The ERA-Interim reanalysis: Configuration and performance of the data assimilation system, *Q. J. R. Meteorol. Soc.*, *137*, 553–597, doi:10.1002/qj.828.

Dunstone, N. J., D. M. Smith, B. B. B. Booth, L. Hermanson, and R. Eade (2013), Anthropogenic aerosol forcing of Atlantic tropical storms, *Nat. Geosci.*, *6*, 534–539, doi:10.1038/ngeo1854.

England, M. H., S. McGregor, P. Spence, G. A. Meehl, A. Timmermann, W. Cai, A. S. Gupta, M. J. McPhaden, A. Purich, and A. Santoso (2014), Recent intensification of wind-driven circulation in the Pacific and the ongoing warming hiatus, *Nat. Climate Change*, *4*, 222–227, doi:10.1038/nclimate2106.

Fyfe, J., et al. (2016), Making sense of the early-2000s warming slowdown, *Nat. Climate Change*, *6*, 224–228, doi:10.1038/nclimate2938.

Govindasamy, B., and K. Caldeira (2000), Geoengineering Earth's radiation balance to mitigate $CO_2$-induced climate change, *Geophys. Res. Lett.*, *27*, 2141–2144, doi:10.1029/1999GL006086.

Govindasamy, B., S. Thompson, P. B. Duffy, K. Caldeira, and C. Delire (2002), Impact of geoengineering schemes on the terrestrial biosphere, *Geophys. Res. Lett.*, *29*, 2061, doi:10.1029/2002GL015911.

Govindasamy, B., K. Caldeira, and P. B. Duffy (2003), Geoengineering Earth's radiation balance to mitigate climate change from a quadrupling of $CO_2$, *Global Planet. Change*, *37*, 157–168, doi:10.1016/S0921-8181(02)00195-9.

Hansen, J., M. Sato, P. Kharecha, and K. von Schuckmann (2011), Earth's energy imbalance and implications, *Atmos. Chem. Phys.*, *11*, 13,421–13,449, doi:10.5194/acp-11-13421-2011.

Jaffe, D., T. Anderson, D. Covert, R. Kotchenruther, B. Trost, J. Danielson, W. Simpson, and T. Berntsen (1999), Transport of Asian air pollution to North America, *Geophys. Res. Lett.*, *6*, 711–714, doi:10.1029/1999GL900100.

Kalidindi, S., B. Govindasamy, A. Modak, and K. Caldeira (2015), Modeling of solar radiation management: A comparison of simulations using reduced solar constant and stratospheric sulphate aerosols, *Clim. Dyn.*, *44*, 2909–2925, doi:10.1007/s00382-014-2240-3.

Kang, S. M., I. M. Held, D. M. W. Frierson, and M. Zhao (2008), The response of the ITCZ to extratropical thermal forcing: Idealized slab-ocean experiments with a GCM, *J. Clim.*, *21*, 3521–3532, doi:10.1175/2007JCLI2146.1.

Karl, T. R., A. Arguez, B. Huang, J. H. Lawrimore, J. R. McMahon, M. J. Menne, T. C. Peterson, R. S. Vose, and H.-M. Zhang (2015), Possible artifacts of data biases in the recent global surface warming hiatus, *Science*, *348*, 1469–1472, doi:10.1126/science.aaa5632.

Kinne, S., et al. (2013), MAC-v1: A new global aerosol climatology for climate studies, *J. Adv. Model Earth Sy.*, *5*, 1–37, doi:10.1002/jame.20035.

Kosaka, Y., and S. P. Xie (2013), Recent global-warming hiatus tied to equatorial Pacific surface cooling, *Nature*, *501*, 403–407, doi:10.1038/nature12534.

Kravitz, B., et al. (2013), Climate model response from the Geoengineering Model Intercomparison Project (GeoMIP), *J. Geophys. Res. Atmos.*, *118*, 8320–8331, doi:10.1002/jgrd.50646.

Liu, H., D. J. Jacob, I. Bey, R. M. Yantosca, and B. N. Duncan (2003), Transport pathways for Asian pollution outflow over the Pacific: Interannual and seasonal variations, *J. Geophys. Res.*, *108*(D20), 8786, doi:10.1029/2002JD003102.

Markowicz, K. M., P. J. Flatau, P. K. Quinn, C. M. Carrico, M. K. Flatau, A. M. Vogelmann, D. Bates, M. Liu, and M. J. Rood (2003), Influence of relative humidity on aerosol radiative forcing: An ACE-Asia experiment perspective, *J. Geophys. Res.*, *108*(D23), 8662, doi:10.1029/2002jd003066.

Matthews, H. D., and K. Caldeira (2007), Transient climate-carbon simulations of planetary geoengineering, *Proc. Natl. Acad. Sci. U.S.A.*, *104*, 9949–9954, doi:10.1073/pnas.0700419104.

Meehl, G. A., H. Teng, and G. Branstator (2006), Future changes of El Niño in two global coupled climate models, *Clim. Dyn.*, *26*, 549–566, doi:10.1007/s00382-005-0098-0.

Meehl, G. A., J. M. Arblaster, J. T. Fasullo, A. Hu, and K. E. Trenberth (2011), Model-based evidence of deep-ocean heat uptake during surface-temperature hiatus periods, *Nat. Climate Change*, *1*, 360–364, doi:10.1038/nclimate1229.

Meehl, G. A., A. Hu, J. M. Arblaster, J. T. Fasullo, and K. E. Trenberth (2013), Externally forced and internally generated decadal climate variability associated with the inderdecadal Pacific oscillation, *J. Clim.*, *26*, 7298–7310, doi:10.1175/jcli-d-12-00548.1.

Mitchell, J. F. B., T. C. Johns, J. M. Gregory, and S. F. B. Tett (1995), Climate response to increasing levels of greenhouse gases and sulphate aerosols, *Nature*, *376*, 501–504, doi:10.1038/376501a0.

Ramanathan, V., et al. (2001), Indian Ocean experiment: An integrated analysis of the climate forcing and effects of the great Indo-Asian haze, *J. Geophys. Res.*, *106*, 28,371–28,398, doi:10.1029/2001JD900133.

Santer, B. D., T. K. Taylor, T. M. L. Wigley, J. E. Penner, P. D. Jones, and U. Cubasch (1995), Towards the detection and attribution of an anthropogenic effect on climate, *Clim. Dyn.*, *12*, 77–100, doi:10.1007/bf00223722.

Smith, S. J., J. van Aardenne, Z. Klimont, R. J. Andres, A. Volke, and S. D. Arias (2011), Anthropogenic sulfur dioxide emissions: 1850–2005, *Atmos. Chem. Phys.*, *11*, 1101–1116, doi:10.5194/acp-11-1101-2011.

Takahashi, C., and M. Watanabe (2016), Pacific trade winds accelerated by aerosol forcing over the past two decades, *Nat. Climate Change*, *6*, 768–772, doi:10.1038/nclimate2996.

Tollefson, J. (2014), The case of the missing heat, *Nature*, *505*, 276–278, doi:10.1038/505276a.

Trenberth, K. E., and J. T. Fasullo (2013), An apparent hiatus in global warming?, *Earth's Future*, doi:10.1002/2013EF000165.

Wang, Y., M. Wang, R. Zhang, S. J. Ghan, Y. Lin, J. Hu, B. Pan, M. Levy, J. H. Jiang, and M. J. Molina (2014), Assessing the effects of anthropogenic aerosols on Pacific storm track using a multiscale global climate model, *Proc. Natl. Acad. Sci. U.S.A.*, *111*, 6894–6899, doi:10.1073/pnas.1403364111.

Wild, M., A. Ohmura, and K. Makowski (2007), Impact of global dimming and brightening on global warming, *Geophys. Res. Lett.*, *34*, L04702, doi:10.1029/2006GL028031.

Xu, Y., and S. Xie (2015), Ocean mediation of tropospheric response to reflecting and adsorbing aerosols, *Atmos. Chem. Phys.*, *15*, 5827–5833, doi:10.5194/acp-15-5827-2015.

Yabe, T., R. Höller, S. Tohno, and M. Kasahara (2003), An aerosol climatology at Kyoto: Observed local radiative forcing and columnar optical properties, *J. Appl. Meteorol.*, *42*, 841–850, doi:10.1175/1520-0450(2003)042.

Yang, T., H. Liao, and S. Lou (2015), Decadal trend and interannual variation of outflow of aerosols from East Asia: Roles of variations in meteorological parameters and emissions, *Atmos. Environ.*, *100*, 141–153, doi:10.1016/j.atmosenv.2014.11.004.